Article

Simulation of Standby Efficiency Improvement for a Line Level Control Resonant Converter Based on Solar Power Systems

Ming-Tse Kuo * and Ming-Chang Tsou

Department of Electrical Engineering, National Taiwan University of Science and Technology, No. 43, Section 4, Keelung Road, Da'an District, Taipei 106, Taiwan; E-Mail: ming@leadtrend.com.tw

* Author to whom correspondence should be addressed; E-Mail: mkuo@mail.ntust.edu.tw; Tel.: +886-2-2730-3288; Fax: +886-2-2737-6699.

Abstract: This paper proposes a new scheme to improve the standby efficiency of the high-power half-bridge line level control (LLC) resonant converter. This new circuit is applicable to improving the efficiency of the renewable energy generation system in distributed power systems. The main purpose is to achieve high-efficiency solar and wind power and stable output under different load conditions. In comparison with the traditional one, this novel method can improve standby efficiency at standby. The system characteristics of this proposed method have been analyzed through detailed simulations, which prove its feasibility.

Keywords: line level control (LLC) resonant converter; holdup time; standby efficiency; distributed generation (DG)

1. Introduction

In most countries, the traditional power-supply system is dominated by large power generators that deliver electricity to each client through the power grid. However, energy supply sources should not rely merely on fuel because of the increasing energy crisis. If a portion of a household's electricity is supplied by way of renewable energy, shortfalls can be covered by electricity companies; when there is surplus renewable energy, it can be fed back into the power grid, adding to the energy supply. Additionally, if most of the households are equipped with recovery apparatus for renewable energy to

reduce power consumption, the power company can also minimize the amount of fossil fuel required to satisfy the load capacity and thereby control environmental pollution. Small distributed generation (DG) systems can generally be categorized into three types, as shown in Figure 1. The first type is the grid-connection system [1]. The power provided by solar power modules is delivered to the load, and excess electricity can be fed into power grid; when the locally provided power is insufficient, the power grid compensates for the inadequacy. The second type is the stand-alone system [2]. Solar or wind power is often treated as renewable energy resource. For example, solar power can charge batteries for contingent use with excess energy; when the electricity from solar power cannot meet the immediate power demand, batteries back up the power insufficiency. Third, there is the hybrid system that combines these two types [3,4]. When the power grid is normal, it functions as a grid-connection system; when there is some interference with the power grid, it becomes a stand-alone system.
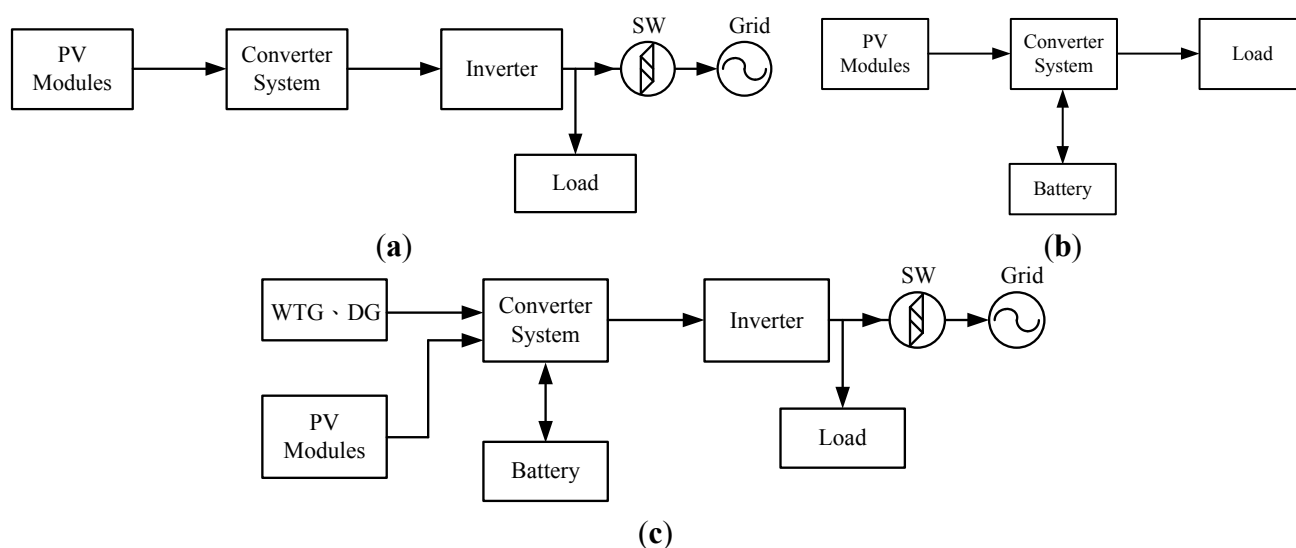
Figure 1. Classification of small generation systems with renewable energy: (**a**) grid-connection system; (**b**) stand-alone system; and (**c**) hybrid system. PV: photovoltaic; WTG: wind turbine generator; DG: distributed generation; and SW: switch.

The development of distributed power systems and renewable energy generation makes power converters an important interface [5]. Taking an independent wind power generation system (Figure 2) as an example, wind turbines generate AC input which is rectified into DC for a line level control (LLC) converter system. Then it supplies energy to load demand and charge batteries. Although LLC converters have high conversion efficiency under heavy load condition, the large switching loss of LLC converters still results in poor standby power loss; even more, it might consume stored power from batteries in a distributed system [6,7].

The aforementioned conversion systems are adapted for renewable energy power converters, and the limitations of those prior studies are as follows: (1) renewable energy is obtained from natural environment sources, but surely they do not provide a stable energy supply, whereas these prior methods are designed based on situations in which renewable energy can stably carry out its tasks; and (2) LLC converters have issues of standby energy loss, which must be minimized to avoid unnecessary influence on battery energy.
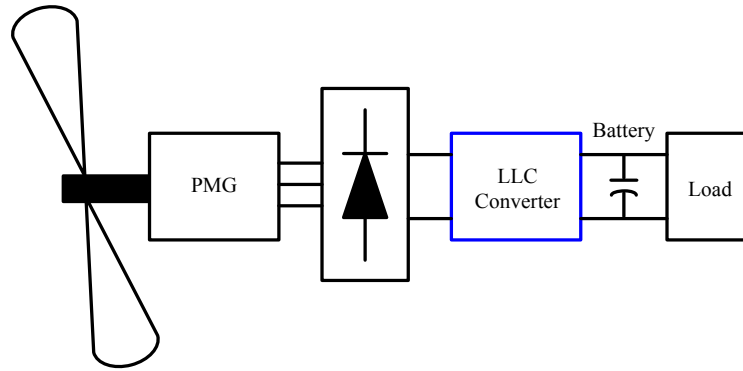
Figure 2. Stand-alone distributed wind power generation system. PMG: permanent magnet generator; and LLC: line level control.

Among several converter types, the LLC converter is the most popular one because it features a wide input range, high conversion efficiency, and high power density, it has been widely applied as a DC/DC power converter [8–10]. For common applications, LLC converters feature high full-load efficiency but provide poor system efficiency during standby because of their large switching losses. They are also compatible with daily-increasing stringent energy regulations and provide fabulous standby efficiency [11–14].

The novel idea of controlling an LLC converter proposed in this paper can reduce the switching losses during standby and allow a wider input range. Under situations with an unstable input source, it can maintain a relatively long period of normal output. The following sections discuss the features and operation principles of this proposed control scheme.

2. Conventional Schemes

The circuit of a typical LLC resonant converter is shown in Figure 3. Its control circuit contains a voltage detector, voltage control oscillator (VCO), and dead-time generator. During this control flow, the partial voltage on the output side receives a voltage feedback signal from the voltage detector. It is then transmitted to the VCO to generate a switching frequency corresponding to the voltage feedback signal, and the dead-time generator generates the dead-time interval to send the switching frequency signal to the power switches. When the output partial voltage is greater than the reference voltage, the voltage detector outputs a relatively high output signal to VCO to push it to generate a correspondingly higher switching frequency; on the other hand, when the divided voltage is smaller than the reference voltage, the voltage detector delivers a relatively low output signal to VCO generating a lower switching frequency. The influence of the switching frequency during standby is highly significant, and therefore how to deal with it in an appropriate control scheme becomes an indispensable need.

To facilitate the analysis, we can transform an LLC resonant converter into a primary-side equivalent model. As shown in Figure 4, from this equivalent model, the transfer function is derived as shown in Equation (1):

$$G(\omega) = \left| \frac{1}{\frac{1}{k}\left(\frac{\omega_{r1}^2}{\omega_{r2}^2} - \frac{\omega_{r1}^2}{\omega_s^2}\right) + jQ_r\left(\frac{\omega_s}{\omega_{r1}} - \frac{\omega_{r1}}{\omega_s}\right)} \right| \tag{1}$$

where $Q_r = \frac{\sqrt{\frac{L_r}{C_r}}}{R_o}$ is the Q-factor, $k = \frac{L_m}{L_r}$ is the ratio between magnetizing inductance and leakage inductance, $\omega_{r1} = \frac{1}{\sqrt{L_r C_r}}$ is the first resonance frequency, and $\omega_{r2} = \frac{1}{\sqrt{(L_r + L_m)C_r}}$ is the second resonance frequency.
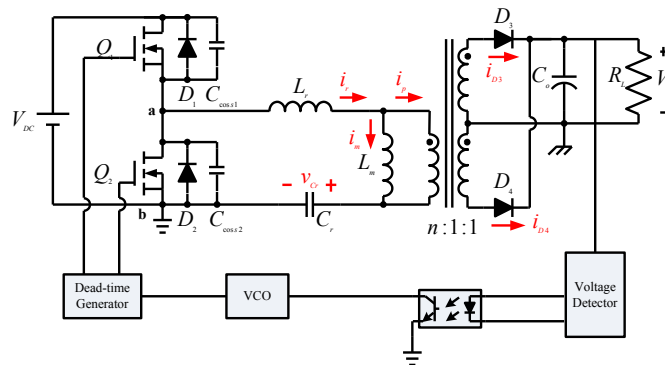
Figure 3. Schematic of LLC resonant converter with basic functional blocks. VCO: voltage control oscillator.
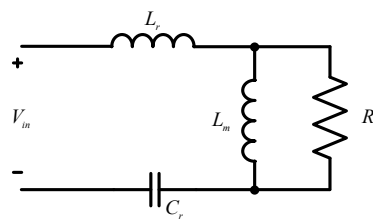
Figure 4. Primary-side equivalent model of LLC resonant converter.

Equation (1) is plotted as the characteristic curve of voltage gain relative to frequency, as shown in Figure 5. By means of two resonant frequencies of ω_{r1} and ω_{r2}, it can designate three regions: (1) Region 1 is the zero voltage switching (ZVS) region in the right half-plane of ω_{r1}; (2) Region 2 is the ZVS region between ω_{r1} and ω_{r2}; and (3) Region 3 is the zero current switching (ZCS) region in the left half-plane of ω_{r2}.
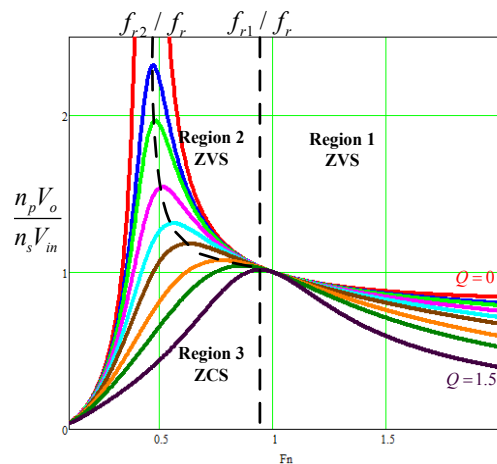
Figure 5. Characteristic curves of voltage gain of LLC resonant converter with respect to frequency.

Metal-oxide-semiconductor field-effect transistor (MOSFET) operation performs relatively well in ZVS mode, and therefore LLC resonant converters mostly work in Regions 1 and 2.

2.1. Operation of the Line Level Control Resonant Converter in Region 1 (Zero Voltage Switching)

The waveform when switching frequency is located at Region 1, as shown in Figure 6. In this region, the magnetizing inductance L_m is clamped by the output voltage, and the entire duty cycle L_m is not included in the resonance. Therefore, the operation mode at this condition acts similar to SRC with ZVS characteristics.
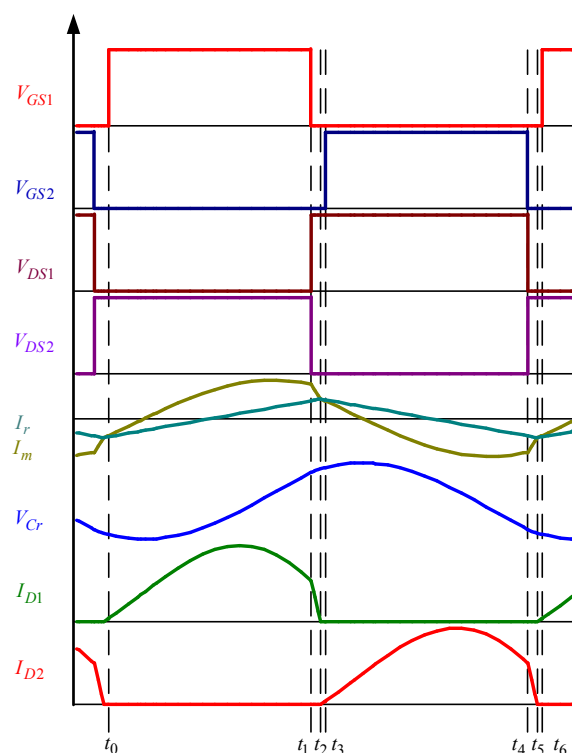
Figure 6. Schematic diagram of LLC resonant converter operated in Region 1 (zero voltage switching, ZVS).

2.2. Operation of the Line Level Control Resonant Converter in Region 2 (Zero Voltage Switching)

When the switching frequency is located in Region 2, the waveform is shown in Figure 7. The resonance in this region is divided into two stages. In the first stage t_0–t_3, the magnetizing inductance L_m is clamped by the output voltage, with L_m non-inclusive in resonance, and the resonant inductance L_r resonates with capacitor C_r; in the second stage t_3–t_4, when the resonant current i_r is equal to the side magnetizing inductance current i_{Lm}, there is no current flowing into transformer, and the secondary side of the converter is tantamount to an open circuit when the magnetizing inductance L_m will resonate with the resonant inductance L_r and the resonant capacitor C_r. Because Region 2 has two resonance frequencies, it is a multi-resonant converter.

The control mode of typical LLC converters is that the output voltage provides feedback to VCO to adjust output power by changing the switching frequency. However, shortcoming of LLC converters is the inferior standby efficiency and relatively high output voltage during no-load. Thus, it causes

no-load switching frequency increases to two to four times than full-load switching frequency, and results in double switching loss.
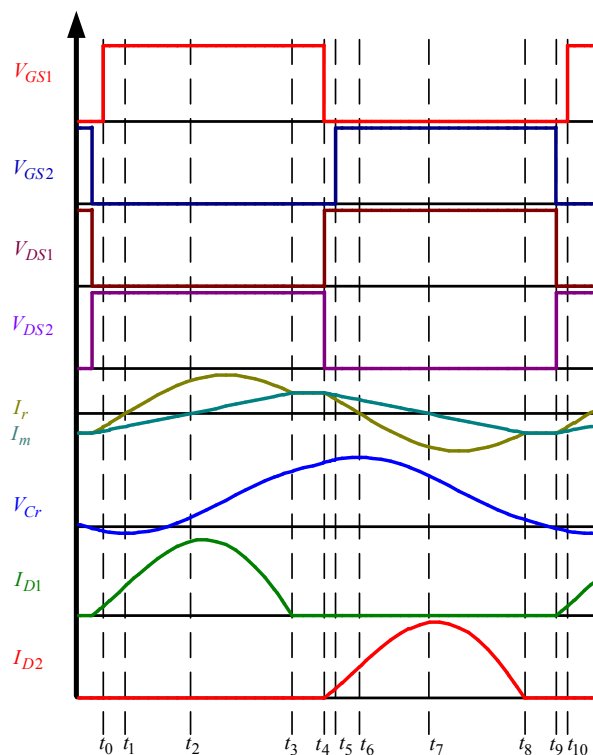
Figure 7. Schematic diagram of LLC resonant converter operated in the mode of Region 2 (ZVS).

To solve the issue of high switching frequency and low efficiency of LLC resonant converters operated at standby, a large number of studies have focused on how to improve standby efficiency, such as burst mode, output saturation inductance, and dummy load regulation. The mostly common approach is burst mode control.

When entering burst mode, it blocks the original high-frequency switching signal by the control circuit, causing episodic high-frequency switching frequency and reducing unnecessary switching loss. Figure 8 shows the burst mode schematics.
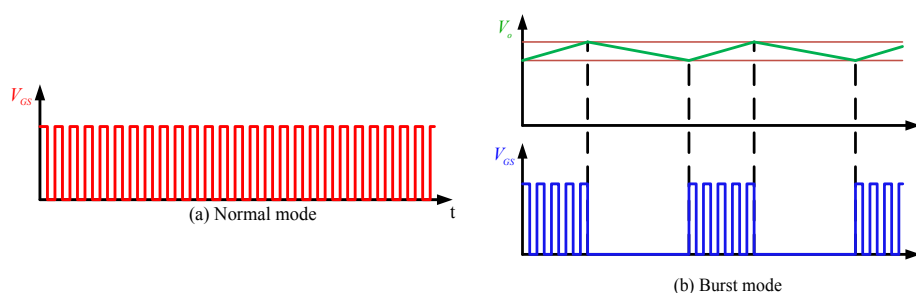
Figure 8. Diagram of burst mode: (**a**) normal mode; and (**b**) burst mode.

The typical control block diagram is shown in Figure 9, and the output signal of VCO sent to logic circuits determines time interval for the switching signal needing masked. However, the drawback is that ripples grow relatively large, and prone to generating audio noise.
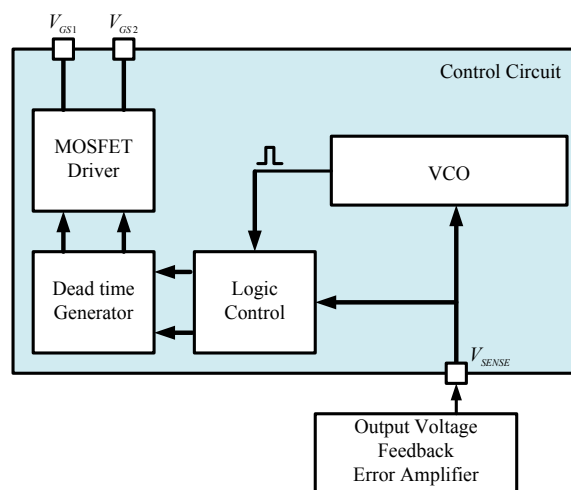
Figure 9. Block diagram of typical control circuit with burst mode. MOSFET: metal-oxide-semiconductor field-effect transistor.

In the next section, SIMPLIS simulation supports establishing behaviors of a typical LLC circuit. For the purpose of making simulation results match the real circuit, the simulated system needs to take parasitic devices into consideration, which probably affects the resonant frequency and voltage gain, and parasitic capacitance especially affects the operating frequency. To simplify the analysis and make simulation converged easily, the revised paper moves all secondary parasitic capacitance to primary side and merges overall parasitic capacitance as equivalent parallel capacitance C_P [11].

Simulation condition 1: Figure 10 shows simulated waveforms of a typical LLC circuit under 480 W/48 V, which adopts VCO to adjust the power. Therefore, the switching frequency varies with load.

(**a**)   (**b**)
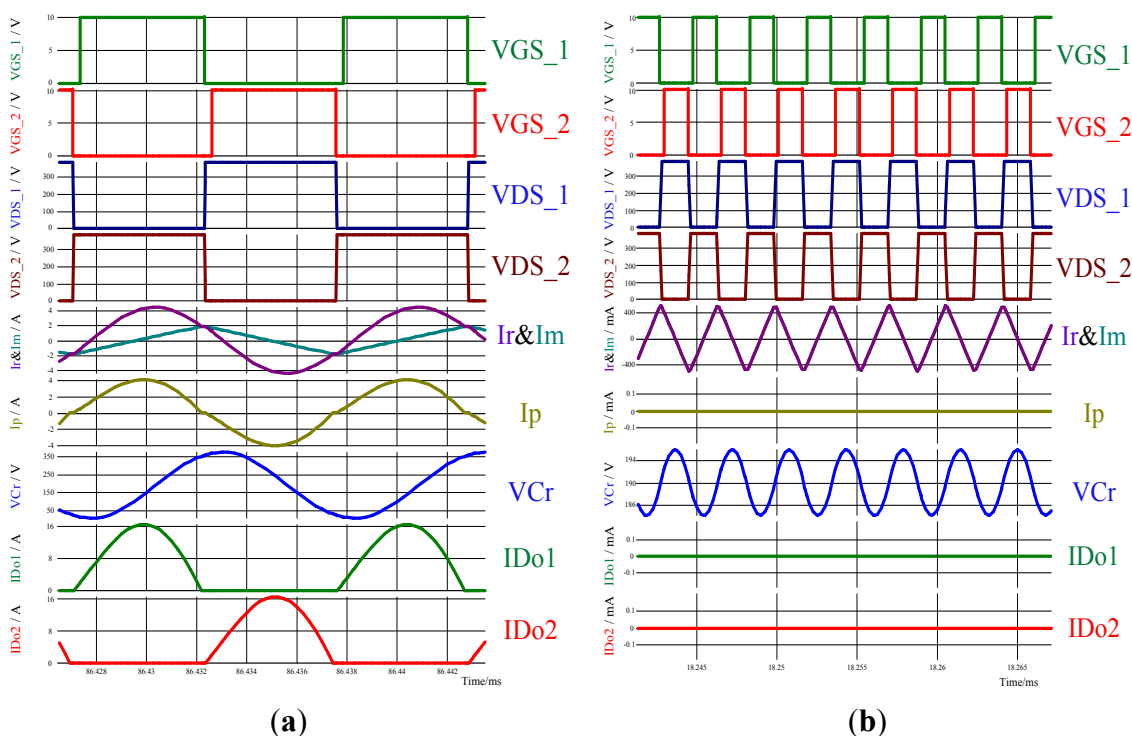
Figure 10. Simulation waveforms for typical LLC circuit at 480 W/48 V: (**a**) 100% load; and (**b**) 0% load.

Simulation condition 2: to observe differences between middle and high power, typical LLC circuit for 1200 W/48 V plays the role of comparable prototype. Figure 11 shows simulations waveform of 1200 W/48 V.
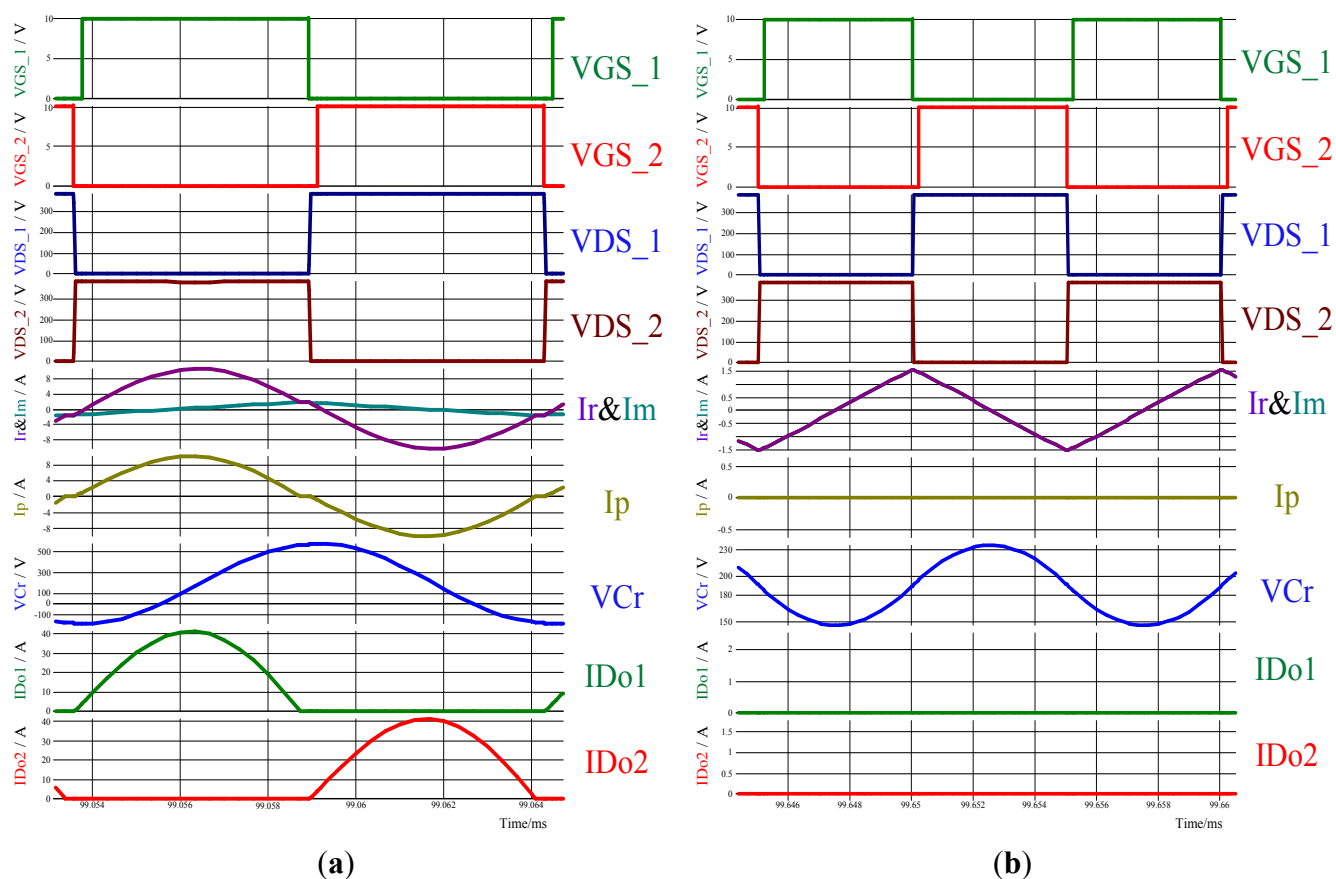
Figure 11. Simulation waveforms for a typical LLC circuit at 1200 W/48 V: (**a**) 100% load; and (**b**) 0% load.

This section describes the operation principles of typical LLC circuits and provides some analysis for different loads. It shows that switching frequency at standby is approximately twice than full-load switching frequency.

3. Novel Line Level Control Circuit

To solve problems of high switching loss upon standby, a novel LLC control circuit is proposed as shown in Figure 12.

When the proposed circuit operates in full-load, the power switch Q_3 of the auxiliary control circuit can be synchronously conducted with the frequency of the primary oscillator and stops as it reaches the condition of the feedback signal of output voltage, which causes the auxiliary switch Q_3 operating with the synchronized pulse-width-modulation (PWM) mode. If the load declines, the duty cycle of the auxiliary switch also decreases; when operated in no-load situations, the duty cycle of the auxiliary switch Q_3 is equal to 0, and makes Q_3 closed. Figure 13 plots main waveforms when the new LLC control circuit operates in full-load situations, which can be divided into four working states.
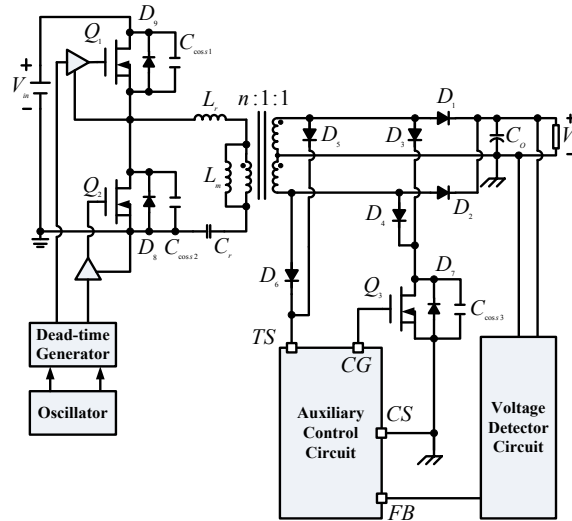
Figure 12. Structural diagram of a novel LLC control circuit.
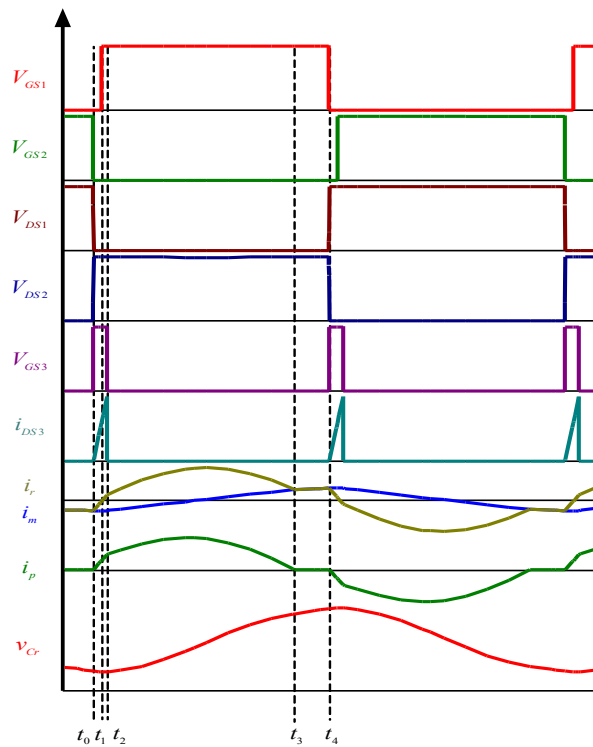
Figure 13. Main waveforms of novel LLC control circuit.

3.1. Working State 1 ($t_0 \leq t \leq t_1$)

In Working State 1, shown in Figure 14, the upper-bridge switch parasitic capacitor C_{coss1} has been discharged to zero, whereas the voltage of the lower-bridge parasitic capacitor C_{coss2}, V_{DS2}, has been charged from 0 to V_{in}. The upper-bridge parasitic diode D_9 is conducted, reaching the condition for the ZVS of the upper-bridge switch Q_1. The auxiliary switch Q_3 is synchronously conducted along with the state transfer of V_{DS2}. At this time, the circuit is operated in the current enhancement mode, and the secondary converter is shorted out by auxiliary switch Q_3. No energy is delivered to the load end, and the energy for the load is provided by the output capacitor C_o. Because the secondary converter is

shorted out, the voltage over the two ends of the magnetizing inductance L_m is clamped at zero, and the magnetizing current i_m is maintained at $i_m(t_0)$ without changing. The voltage across the resonant inductance L_r also increases due to the secondary short circuit when only the resonant inductance L_r and resonant capacitor C_r participate in resonance. However, due to the secondary short circuit, the resonant circuit $i_r(t)$ is forced to undergo a relatively rapid linear increase. At $t = t_1$, the upper-bridge switch Q_1 is conducted to complete the zero-voltage switching. At this instant, the resonant current $i_r(t)$ increases to zero, and this mode ends.
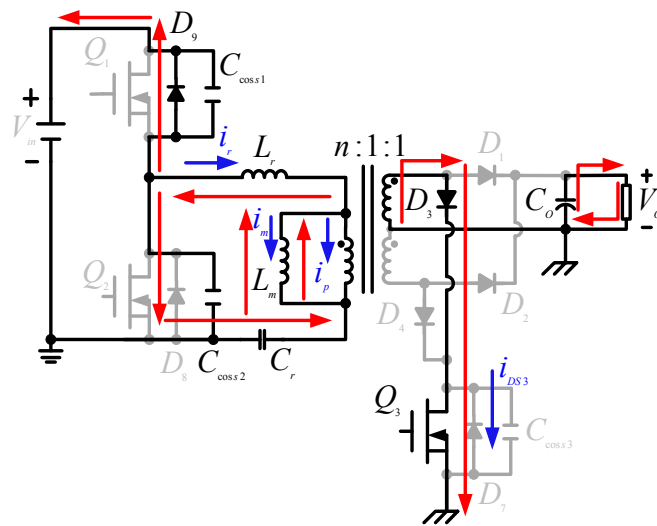
Figure 14. Working State 1 of novel LLC control circuit.

3.2. Working State 2 (t₁ ≤ t ≤ t₂)

In this working state, the two ends of magnetizing inductance L_m are still clamped at zero by the secondary short circuit, and the magnetizing current i_m is maintained at $i_m(t_0)$ without changing; at this time, only the resonant inductance L_r and resonant capacitance C_r participate in the resonance, whereas the resonant current i_r continues to undergo a rapid linear increase. The state of the circuit is shown in Figure 15. At $t = t_2$, the auxiliary circuit stops the auxiliary switch Q_3, and this mode ends.
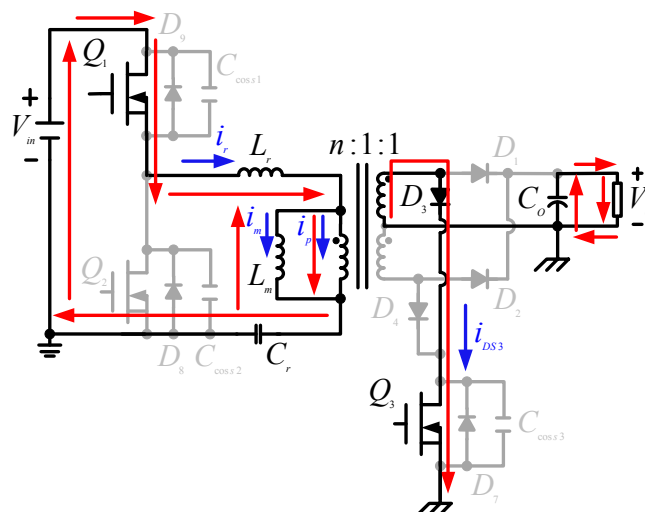
Figure 15. Working State 2 of novel LLC control circuit.

3.3. Working State 3 (t₂ ≤ t ≤ t₃)

In Working State 3, shown in Figure 16, the two ends of the magnetizing inductance L_m are clamped at nV_o by the output voltage, and therefore, the magnetizing current i_m continues to increase linearly; only the resonant inductance L_r and the resonant capacitor C_r still participate in the resonance, but the resonant current i_r restores to increase as a sinusoidal waveform. When $t = t_3$, the resonant current i_r is equal to the magnetizing current i_m. The current through the output rectifier diode D_1, i_{D1}, resonates to zero and stops, completing ZCS, and this mode is over.
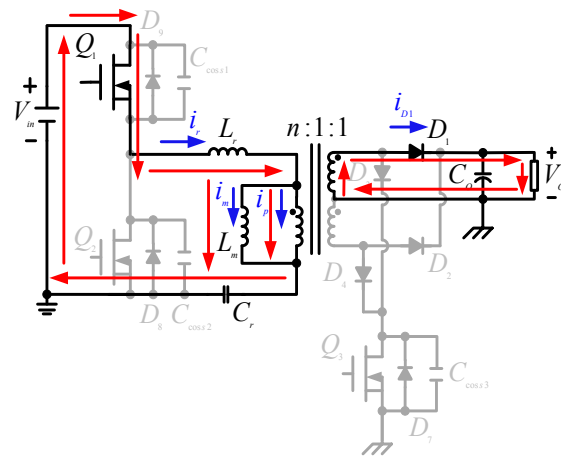
Figure 16. Working State 3 of novel LLC control circuit.

3.4. Working State 4 (t₃ ≤ t ≤ t₄)

In Working State 4 in Figure 17, because the output rectifier diode is turned off, the power on the input end cannot be delivered to the secondary load, and the converter is in the decoupled state. At this time, the resonant inductance L_r and resonant capacitance C_r resonate with the magnetizing inductance L_m; because the magnetizing inductance L_m is much larger than the resonant inductance L_r, the resonance frequency decreases, and the resonant current waveforms i_r becomes relatively flat. Because the resonant current through the resonant inductance L_r, i_r, is continuous, the resonant current i_r continues to charge the resonant capacitor C_r. At $t = t_4$, upper-bridge switch Q_1 turns off, and this state ends.
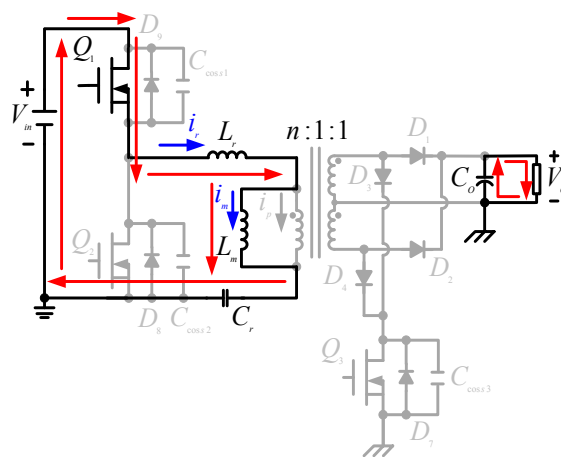
Figure 17. Working State 4 of novel LLC control circuit.

Now that operation principles is clarified, first presume that input voltage V_o and output voltage V_o are both constant in one switching period. Furthermore, to simplify analysis, assume that the magnetizing inductance L_m is very large, and therefore magnetizing current i_m is zero. It can be derived that the equation for voltage gain is given by Equation (2):

$$\frac{nV_o}{\frac{V_{in}}{2}} = \frac{\frac{T_s}{C_r R_{ac}} + \sqrt{\left(\frac{T_s}{C_r R_{ac}}\right)^2 + 4\left[1 - \cos^2\left(\omega_{r1}\frac{DT_s}{2}\right)\right]\frac{T_s}{C_r R_{ac}}}}{2n\left[1 + \cos\left(\omega_{r1}\frac{DT_s}{2}\right)\right]\frac{T_s}{C_r R_{ac}}} \quad (2)$$

Voltage gain curves are plotted based on above equations, as shown in Figure 18. It indicates the auxiliary switch Q_3 plays a role in increasing resonant current i_r. Along with the duty cycle D of auxiliary switch Q_3 increasing, higher voltage gains can be obtained.
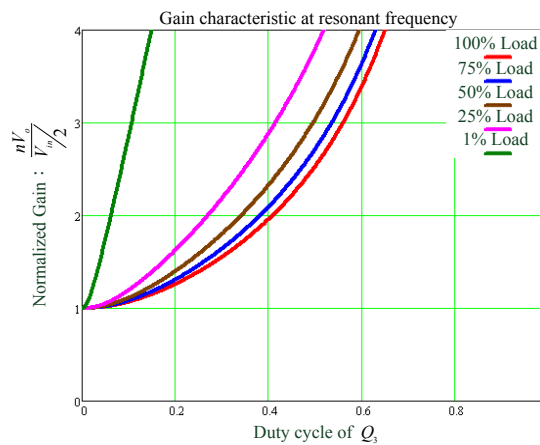
Figure 18. Characteristic plots of system gain that changes with load.

From the perspective of the resonant tank, Figure 19 shows the characteristic relationship curve between resonant tank parameters and system gain with fixed magnetizing inductance. Moreover, it also indicates the lower resonant inductance L_r induces the higher system gain during the same operation period D. It means that the lower design resonant inductance L_r adopts, the higher current gain the system gets.
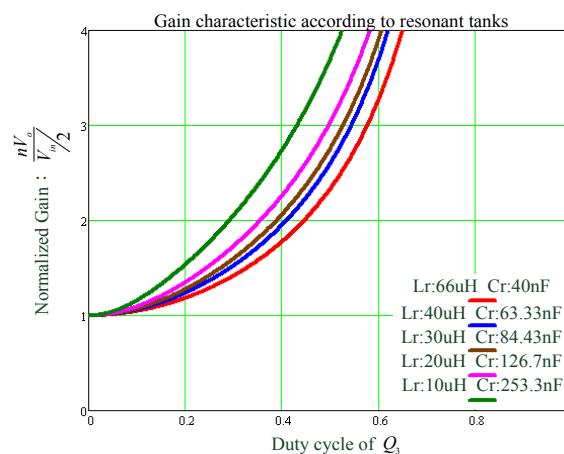
Figure 19. Characteristic plots of system gain changing with resonant tank.

By means of the auxiliary control circuit shown in Figure 20, the above functions are achieved, and the auxiliary control circuit also has the function of sequential detection and voltage detection.
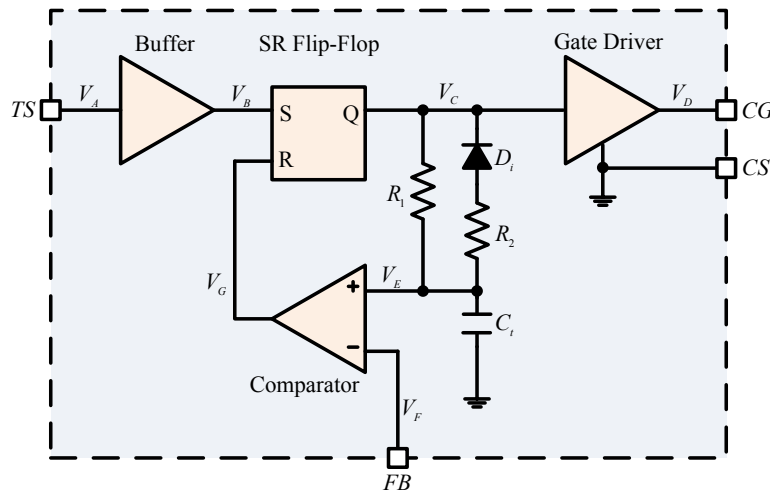
Figure 20. Block diagram of auxiliary control circuit.

Figure 21 shows waveforms of the auxiliary control circuit.
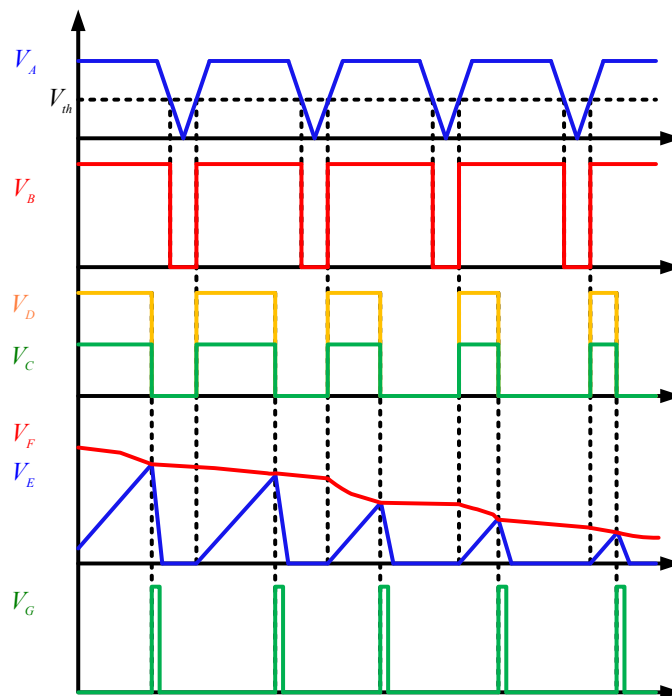
Figure 21. Principle waveforms of auxiliary control circuit.

The next section will report simulation results and analysis for novel LLC control circuits.

4. Simulation Results and Analysis

Based on the theoretical analysis above, feasibility of the method proposed in this paper can be verified with the help of SIMPLIS simulation, and the performances acquired by simulation obviously demonstrates it getting overwhelming superior positions in comparison of conventional type circuit:

(1) The simulated circuit and function block diagram are built and behaves following proposed operation principles truly, as shown in Figure 22.
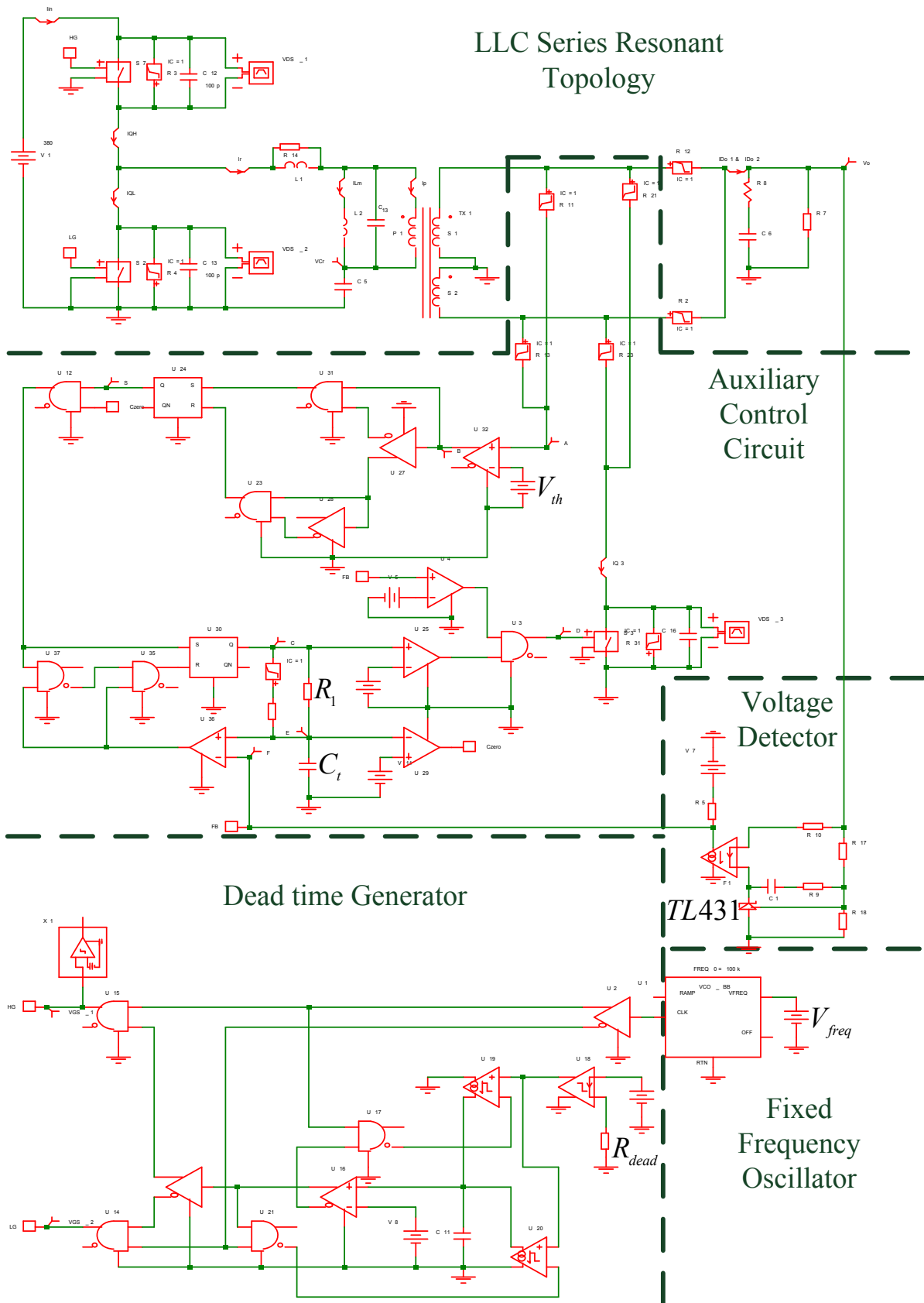
Figure 22. Novel LLC simulation circuit.

Simulation condition 3 (novel LLC control circuit): P_{omax} = 480 W, V_{o} = 48 V, L_{m} = 264 µH, L_{r} = 30 µH, C_{r} = 100 nF, and C_{P} = 12.28 nF.

Simulation condition 4 (novel LLC control circuit): P_{omax} = 1200 W, V_{o} = 48 V, L_{m} = 264 µH, L_{r} = 20 µH, C_{r} = 130 nF, and C_{P} = 30.72 nF.

Table 1 lists simulation result comparisons between the novel LLC control circuits and typical LLC circuits. This table shows that switching frequency of typical LLC resonant converters at standby tends to reach even twice than that at full-load, whereas the novel LLC control circuit still operates at fixed frequency regardless of whether in standby or full-load conditions. By attributions from power switch of the auxiliary control circuit keeping in cut-off state, switching loss degrades accompanied with a relatively large peak input current, $I_{\text{in\_peak}}$.

Table 1. Comparison between the simulation results for typical LLC circuit and new LLC circuit.

480 W/48 V@100% load	f_{SW}	$I_{\text{in\_peak}}$		f_{Q3}
Conventional LLC	98.89 kHz	4.521 A		N/A
Proposed LLC	99 kHz	6.827 A		198 kHz
480 W/48 V@0% load	f_{SW}	$I_{\text{in\_peak}}$	$I_{\text{in\_rms}}$	f_{Q3}
Conventional LLC	285.15 kHz	0.688 A	0.327 A	N/A
Proposed LLC	95 kHz	1.018 A	0.486 A	0 Hz
1200 W/48 V@100% load	f_{SW}	$I_{\text{in\_peak}}$		f_{Q3}
Conventional LLC	96.52 kHz	12.016 A		N/A
Proposed LLC	96 kHz	23.791 A		186 kHz
1200 W/48 V@0% load	f_{SW}	$I_{\text{in\_peak}}$	$I_{\text{in\_rms}}$	f_{Q3}
Conventional LLC	258.47 kHz	1.810 A	0.824 A	N/A
Proposed LLC	96 kHz	2.360 A	1.076 A	0 Hz

According to the formulas for the LLC resonant converter operated under no load conditions, the dominant power loss is roughly divided into four parts, such as switching loss and conduction loss on power switches, copper loss and core loss on the transformer. Besides, the material of cores and temperature-related parameters on transformers cannot be rebuilt accurately in a simulated system, which makes it not convincing if core loss is taken into consideration in the simulation. Thus, this paper ignores core loss estimation:

$$P_{\text{turn-off\_loss}} = \frac{1}{2} \times V_{\text{DS}} \times I_{\text{DS\_Peak}} \times t_{\text{f}} \times f_{\text{s}} \tag{3}$$

$$P_{\text{conduction\_loss}} = I_{\text{DS\_RMS}} \times R_{\text{DS\_on}} \tag{4}$$

$$P_{\text{core}} = C_{\text{m}} \times f^{x} \times B_{\text{peak}}^{y} \times (ct_0 - ct_1 \times T + ct_2 \times T^2) \tag{5}$$

$$P_{\text{Copper}} = I_{\text{in\_rms}}^{2} \times R_{\text{pri}} + I_{\text{sec\_rms}}^{2} \times R_{\text{sec}} \tag{6}$$

Proved by Figures 23 and 24 and Tables 1 and 2, LLC systems with the novel control circuit perform better efficiency at standby.
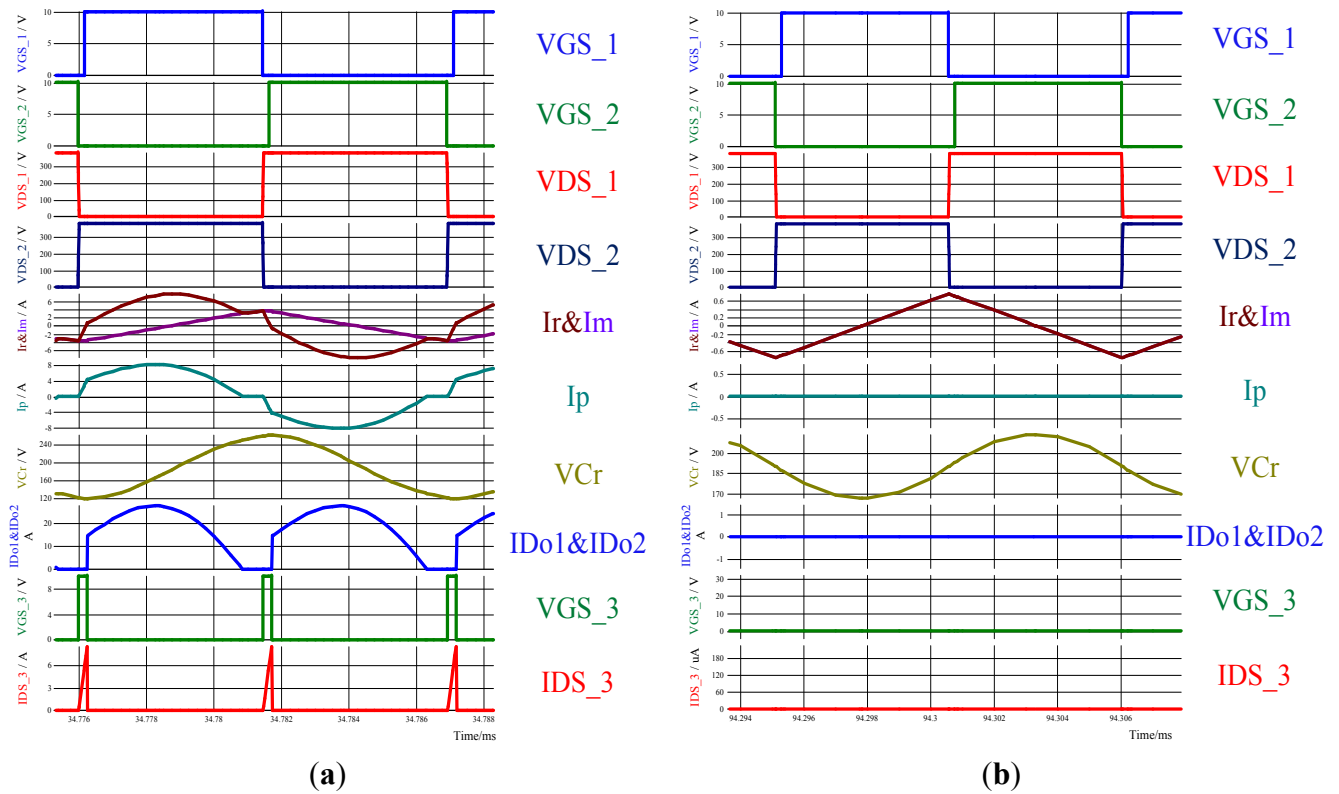
Figure 23. Simulation waveforms for novel LLC control circuit at 480 W/48 V: (**a**) 100% load; and (**b**) 0% load.
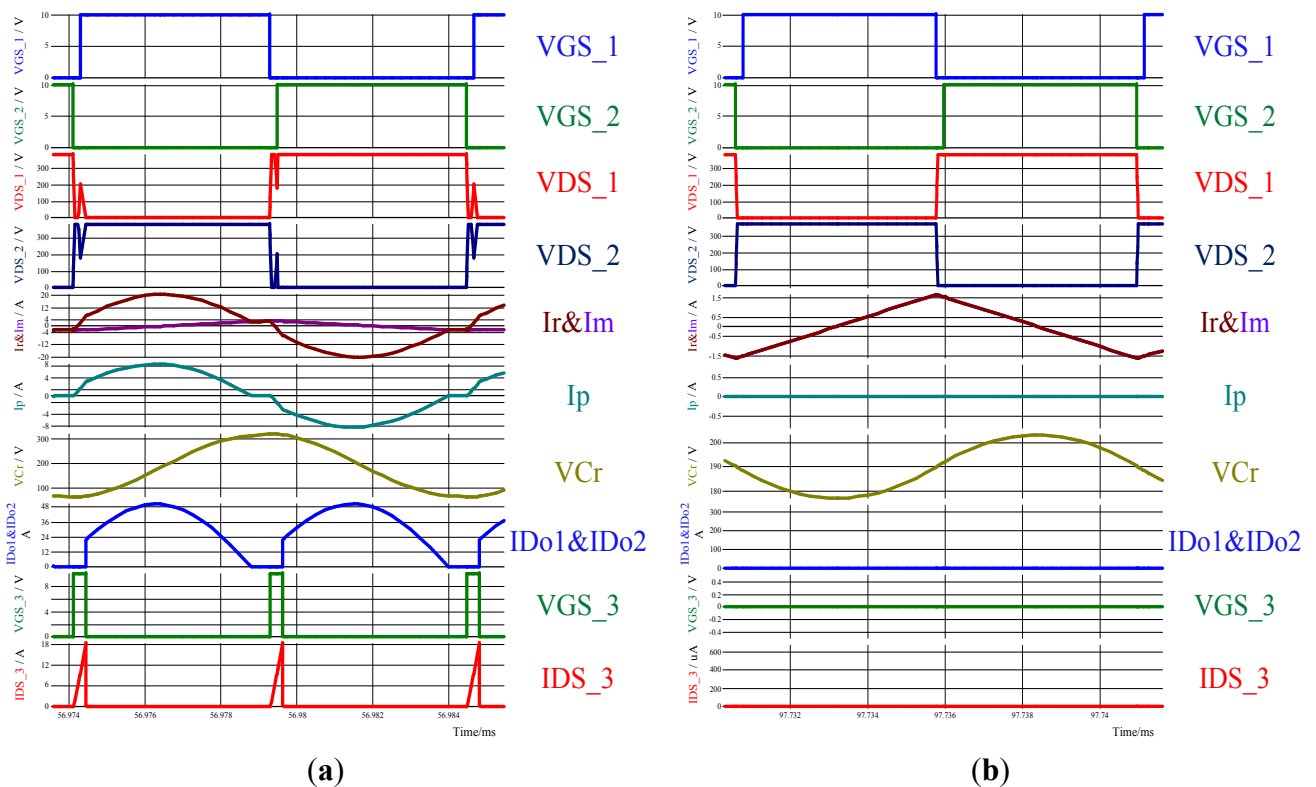
Figure 24. Simulated waveform for typical LLC control circuit under 1200 W/48 V: (**a**) 100% load; and (**b**) 0% load.

Table 2. Overall power loss at standby.

Specification	Type		Conventional LLC	Novel LLC
480 W/48 V	MOS-FDP12N50	R_{pri} 0.2 Ω	2.0305 W	1.1846 W
1200 W/48 V	MOS-FDA28N50	R_{pri} 0.08 Ω	10.9608 W	5.4568 W

5. Conclusions

The purpose of this paper is mainly to focus on renewable energy generation system at standby. A novel control scheme for LLC converters is introduced to optimize switching loss and improve standby efficiency. Features between typical LLC circuit and proposed LLC control circuit get analyzed in detail. From SIMPLIS simulation results and standby power loss evaluation, some overall conclusions can be derived as follows:

(1) Systems with proposed control schemes achieve optimal standby power consumptions.
(2) Even though the magnetizing inductance remains unchanged, the resonant inductance is permitted with a relatively small design, bringing advantages such as smaller volumes of magnetic components and improving power density.
(3) This system can also enhance current gain and operate in a wide input range. The hold-up time increases, which reduces capacitance size and improves power density; additionally, operating range of wind generators gets improved.
(4) The control loop at system input and output side is independent, and therefore, isolation between control circuits is naturally accomplished.

Acknowledgments

Author Contributions

Both of the authors played important roles during the design of standby efficiency improvement and partially wrote the paper. Ming-Chang Tsou ran the simulation and Ming-Tse Kuo reviewed and revised the manuscript.

Conflicts of Interest

The authors declare no conflict of interest.

References

1. Giraud, F.; Salameh, Z.M. Steady-state performance of a grid-connected rooftop hybrid wind-photovoltaic power system with battery storage. *IEEE Trans. Energy Convers.* **2001**, *16*, 1–7.

2. Nehrir, M.H.; LaMeres, B.J.; Venkataramanan, G.; Gerez, V.; Alvarado, L.A. Performance Evaluation of Stand-Alone Wind/Photovoltaic Genera System. In Proceedings of the IEEE Power Engineering Society Summer Meeting, Edmonton, AB, Canada, 18–22 July 1999; Volume 1, pp. 555–559.

3. Park, S.J.; Kang, B.B.; Yoon, J.P.; Cha, I.S.; Lim, J.Y. A Study on the Stand-Alone Operating or Photovoltaic/Wind Power Hybrid Generation System. In Proceedings of the IEEE 35th Annual Power Electronics Specialists Conference, PESC 04, Aachen, Germany, 20–25 June 2004; Volume 3, pp. 2095–2099.

4. Dou, X.; Quan, X.; Wu, Z.; Hu, M.; Sun, J.; Yang, K.; Xu, M. Improved control strategy for microgrid ultracapacitor energy storage systems. *Energies* **2014**, *7*, 8095–8115.

5. Drouilhet, S.; Muljadi, E.; Holz, R.; Gevorgian, V. *Optimizing Small Wind Turbine Performance in Battery Charging Applications*; NREL/TP-441–7808; National Renewable Energy Laboratory (NREL): Golden, CO, USA, 1995.

6. Lee, F.C.; Barbosa, P.; Xu, P.; Zhang, J.; Yang, B.; Canales, F. Topologies and design considerations for distributed power system applications. *Proc. IEEE* **2001**, *89*, 939–950.

7. Krishna, R.A.; Dutt, A.A. LLC Resonant Converter with Renewable Energy Source for Low Voltage Application. In Proceedings of the 2011 International Conference on Signal Processing, Communication, Computing and Networking Technologies (ICSCCN), Thuckafay, India, 21–22 July 2011; pp. 383–388.

8. Yang, B.; Lee, F.C.; Zhang, A.J.; Huang, G.S. LLC Resonant Converter for Front End DC/DC Conversion. In Proceedings of the Seventeenth Annual IEEE Applied Power Electronics Conference and Exposition, APEC 2002, Dallas, TX, USA, 10–14 March 2002; Volume 2, pp. 1108–1112.

9. Yang, B. Topology Investigation for Front End DC/DC Power Conversion for Distributed Power. Ph.D. Thesis, Virginia Tech, Blacksburg, VA, USA, 2003.

10. Fang, Y.; Xu, D.; Zhang, Y.; Gao, F.; Zhu, L.; Chen, Y. Standby Mode Control Circuit Design of LLC Resonant Converter. In Proceedings of the IEEE Power Electronics Specialists Conference, PESC 2007, Orlando, FL, USA, 17–21 June 2007; pp. 726–730.

11. Ye, Y.; Yan, C.; Zeng, J.; Ying, J. A Novel Light Load Solution for LLC Series Resonant Converter. In Proceedings of the 29th International Telecommunications Energy Conference, INTELEC 2007, Rome, Italy, 30 September–4 October 2007; pp. 61–65.

12. Jung, J.-H.; Kwon, J.-G. Theoretical Analysis and Optimal Design of LLC Resonant Converter. In Proceedings of the 2007 European Conference on Power Electronics and Applications, Aalborg, Denmark, 2–5 September 2007; pp. 1–10.

13. Cheng, C.A.; Chen, H.W.; Chang, E.C.; Yen, C.H.; Lin, K.J. Efficiency Study for a 150W LLC Resonant Converter. In Proceedings of the International Conference on Power Electronics and Drive Systems, PEDS 2009, Taipei, Taiwan, 2–5 November 2009; pp. 1261–1265.

14. Kim, B.-C.; Park, K.-B.; Kim, C.-E.; Lee, B.-H.; Moon, G.-W. LLC resonant converter with adaptive link-voltage variation for a high-power-density adapter. *IEEE Trans. Power Electron.* **2010**, *25*, 2248–2252.